Chapter

Electrical Properties of Polypropylene-Based Composites Melt-Processed with As-Grown Carbon Nanofibers

António Jose Paleo, Zineb Samir, Najoia Aribou, Yassine Nioua, Joaquim Agostinho Moreira and Mohammed Essaid Achour

Abstract

Electrical conductivity, dielectric permittivity, electrical modulus, and electrical impedance of polypropylene (PP) composites melt-processed with different contents of as-grown carbon nanofibers (CNFs) are studied. As expected, the electrical conductivity of PP/CNF composites increased as the incorporation of CNFs is raised in the polymer, yielding a maximum of $\sim 6 \times 10^{-6}$ S m^{-1} for PP/CNF 3 wt. % composites. That enhancement relates to a gradual improvement of the dielectric permittivity as the incorporation of CNFs rises into the PP up to a maximum of ~ 13 for PP/CNF 3 wt. % composites at 1MHz, which is attributed to the rise of the interface polarization effect. Moreover, the Cole-Cole model is used through the electrical modulus to analyze the effect of CNF contents on the dielectric relaxation of PP/CNF composites from which is deduced that the incorporation of CNFs increases their heterogeneity and relaxation times. The analysis gathered here aims at contributing to the understanding of the electric features of polymer composites filled with a type of CNFs, which are not subjected to any thermal post-processing method after their synthesis by chemical vapor deposition (CVD).

Keywords: polypropylene, carbon nanofibers, dielectric spectroscopy, electrical modulus, Cole-Cole model

1. Introduction

Polypropylene (PP) is one of the most widely used and low-cost thermoplastics with adequate physical properties, such as low density and high heat resistance [1]. PP is generally found as homopolymer and copolymer. The first one consists of propylene monomers and it has a high strength-to-weight ratio and good chemical resistance. Whereas the second one includes monomers in the PP backbone, and it is tougher and more flexible, with a lower melting point and high-impact resistance at low temperatures than PP homopolymer [2]. Because of all these advantages, polypropylene-based composites have been extensively used for automotive, construction, and packaging applications [3]. In this respect, melt processing is the preferred solution processing in

developing PP-based composites since the production in the melt state permits to obtain large material quantities and prevents the need of using toxic solvents [4]. On the other hand, vapor grown carbon nanofibers (CNFs) are an attractive option among other carbon materials, such as carbon black (CB), carbon nanotubes (CNTs), and graphene, as reinforcing fillers for polypropylene given their large surface area, high strength and storage modulus, and excellent thermal and electrical properties [5]. This type of CNF, which is produced by chemical vapor deposition (CVD) of catalyst nanoparticles under a mixture of gaseous hydrocarbons [6], have tubular hollow cores surrounded by ordered inner stacked-cup and disordered outer layers, with lengths and diameters ranging from 50 to 100 μm, and 50 to 200 nm, respectively [7, 8]. In particular, due to their remarkably electrical conductivities (10^4 S m^{-1}), the production of conductive PP composites based on CNFs by melt-mixing has been the subject of investigation during the past few decades [9–11]. Notably, the broad dispersion of electrical conductivity values reported for melt-processed PP/CNF composites shows that their electrical properties are far from being totally understood [12]. It is in this context that this study is conducted. Specifically, the analysis involving the improved dielectric permittivity of PP composites melt-processed with different contents of as-grown carbon nanofibers [12, 13], which are not subjected to any thermal post-processing method after their CVD synthesis are revisited in this work. The effects of CNFs on the AC electrical conductivity and dielectric permittivity of PP/CNF composites are detailed with the use of the electrical modulus formalism from which the phenomenological Cole-Cole model is utilized. The principal aim is to understand the physics governing the enhanced, quite stable dielectric constants, and low dielectric losses of PP composites melt-processed with this particular type of CNFs.

2. Materials and methods

PR 25 AG carbon nanofibers in the form of powder (ASI, Cedarville, OH, USA) without any chemical modification and polypropylene (Daplen™ Borealis EE002AE) were utilized for producing the PP/CNF composites. The CNFs produced by this company are grown catalytically from gaseous hydrocarbons using metallic catalyst particles [14]. In particular, these PR 25 AG CNFs are not subjected to any thermal post-processing method. They show a structure composed of a hollow core surrounded by two regions with different appearances: an internal region with an oriented and regular structure, and an external region characterized by uneven graphite sheets and amorphous carbon [15, 16]. In terms of dimensions, the CNFs have lengths of 30–100 μm and diameters of 100–200 nm. [6, 15]

The PP/CNF composites were melt-extruded on a modular lab-scale intermeshing mini corotating twin-screw extruder, with a screw diameter of 13 mm, barrel length of 31 cm, and an approximate L/D ratio of 26. The screw configuration was chosen to achieve high shear mixing levels and longer residence times. The screw rotational speed was kept constant at 50 rpm and the barrel temperature was 190°C [17]. The melt-extruded PP/CNF composites were pelletized and compression-molded with the appropriate dimensions for the different analyses. PP/CNF composites with weight concentrations from 0.5 to 3 wt. % were obtained and analyzed.

2.1 Experimental techniques

The morphological analysis of PP/CNF composites was examined by scanning electron microscope (SEM) (JEOL JSM-6400) at an accelerating voltage of 20 kV. The

specimens were broken under cryogenic conditions and then sputter-coated with a thin layer of gold before testing. Infrared measurements (FTIR) (IRAffinity-1S, Shimadzu) were performed in transmission mode from 600 to 2000 cm^{-1} at room temperature. FTIR spectra were collected with 40 scans and resolution of 4 cm^{-1}. Raman spectroscopy measurements (ALPHA300 R Confocal Raman Microscope WITec) were carried out using 532 nm laser for excitation in backscattering geometry. The laser beam with P = 0.5 mW was focused on the sample by a × 50 lens (Zeiss), and the spectra were collected with 600 groove/mm grating using 30 acquisitions with 2 s acquisition time. The X-ray diffraction (XRD) (PANalytical X'Pert Pro diffractometer) equipped with X'Celerator detector and secondary monochromator in θ/2θ Bragg-Brentano geometry was collected at room temperature. The measurements were carried out using a Cu Kα radiation ($\lambda\alpha_1$ =1.54060 Å and $\lambda\alpha_2$ = 1.54443 Å) 40 kV and 30 mA, at a resolution of 0.017° per step, with a 100 s integration per step, over the range 2θ=10-60°.

2.2 Electrical analysis

Squared films of 0.5 × 10 × 10 mm^3 with Au electrodes deposited by thermal evaporation on both sides were utilized for AC electrical analysis. The capacity C and dielectric loss tan δ at room temperature were measured by using a precision meter (Quadtech 1929 LCR) at frequencies between 430 Hz and 2 MHz with an applied signal of 0.5 V. The real $\varepsilon'(\omega)$ and imaginary $\varepsilon''(\omega)$ parts of the complex dielectric permittivity $\varepsilon^*(\omega)$ were calculated by the equations:

$$\varepsilon'(\omega) = C(\omega).{}^{d}\!/_{\varepsilon_0 A} \tag{1}$$

$$\varepsilon''(\omega) = \varepsilon'(\omega) tan\delta(\omega) \tag{2}$$

Here, d is the thickness, A is the surface area (10×10 mm^2), ε_0 is the permittivity of vacuum (8.85×10^{-12} F m^{-1}), and $\omega = 2\pi f$ is the circular frequency. In turn, the real $\sigma'(\omega)$ and imaginary $\sigma''(\omega)$ parts of the complex conductivity $\sigma^*(\omega)$ was obtained by using the following expressions:

$$\sigma'(w) = w\ \varepsilon_0 \varepsilon''(w) \tag{3}$$

$$\sigma''(w) = w\ \varepsilon_0 \varepsilon'(w) \tag{4}$$

The electrical complex modulus $M^*(\omega)$ was calculated by:

$$M^*(\omega) = {}^{1}\!/_{\varepsilon^*(\omega)} = M'(\omega) + iM''(\omega) \tag{5}$$

Here, $M'(\omega)$ and $M''(\omega)$ are the real and imaginary parts of the electrical complex modulus, which can be expressed by using the complex dielectric permittivity [18]:

$$M'(\omega) = {}^{\varepsilon'(\omega)}\!/_{\left(\varepsilon'^2(\omega)+\varepsilon''^2(\omega)\right)} \tag{6}$$

$$M''(\omega) = {}^{\varepsilon''(\omega)}\!/_{\left(\varepsilon'^2(\omega)+\varepsilon''^2(\omega)\right)} \tag{7}$$

The complex impedance $Z^*(\omega)$ was obtained by using the relations [19]:

$$Z^*(\omega) = Z'(\omega) + iZ''(\omega) = -i\omega C_0 \varepsilon^*(\omega) \tag{8}$$

$$Z'(\omega) = {}^{1}\!/_{2\pi f C_0}\left[{}^{\varepsilon''(\omega)}\!/_{\varepsilon'(\omega)+\varepsilon''(\omega)}\right] \tag{9}$$

$$Z''(\omega) = {}^{1}\!/_{2\pi f C_0}\left[{}^{\varepsilon'(\omega)}\!/_{\varepsilon'(\omega)+\varepsilon''(\omega)}\right] \tag{10}$$

Here, $Z'(\omega)$ and $Z''(\omega)$ are the real and imaginary parts of the complex impedance, and C_0 is the capacitance of the vacuum [20].

3. Results and discussions

3.1 Morphological and structural analysis

The SEM micrographs of melt-extruded PP/CNF 2 wt. % composites at low and higher magnifications manifest some predisposition of CNFs to agglomerate (**Figure 1**). It must be noted that the received CNFs labeled as PR 25 AG used in this work are not treated with any debulking method, unlike the Pyrograf®-III CNFs produced by the same company (ASI, Cedarville, OH, USA). This lack of debulking process could explain their worse dispersion in the polymer [17]. Moreover, the PR 25 AG grade is not thermally treated after its production, which results in less graphitized outer layers. Thereby, it is expected that the conducting polymer composites (CPCs) produced with them show lower electric conductivities [21].

The FTIR spectra in the 600–2000 cm^{-1} range at room temperature of melt-extruded PP and PP filled with 1, 2, and 3 wt. % of CNFs is presented (**Figure 2a**). The FTIR of as-received CNFs is not plotted since did not show any transmittance peaks. PP shows characteristic peaks (1377 and1456 cm^{-1}) assigned to CH_3 symmetric and asymmetric bending vibration, respectively [22]. Other bands are found at 1170 cm^{-1} (CH_2 twisting and CH wagging vibration), 998 cm^{-1} (CH bending and wagging vibrations and CH_3 rocking vibration), 973 cm^{-1} (CH_3 rocking, CH_2 wagging, and CH bending vibrations), and at 840 cm^{-1} (CH_2 rocking and C-CH_3 stretching vibrations) [23]. The peaks assigned to the polypropylene are not altered in PP/CNF composites with 1 and 2 wt. % of CNFs. However, the PP/CNF 3 wt. % composite shows an evident broadening in the band located at 1255 cm^{-1} shown by the arrow (**Figure 2a**), which is associated with CH_2 wagging and CH bending vibration in PP [23].

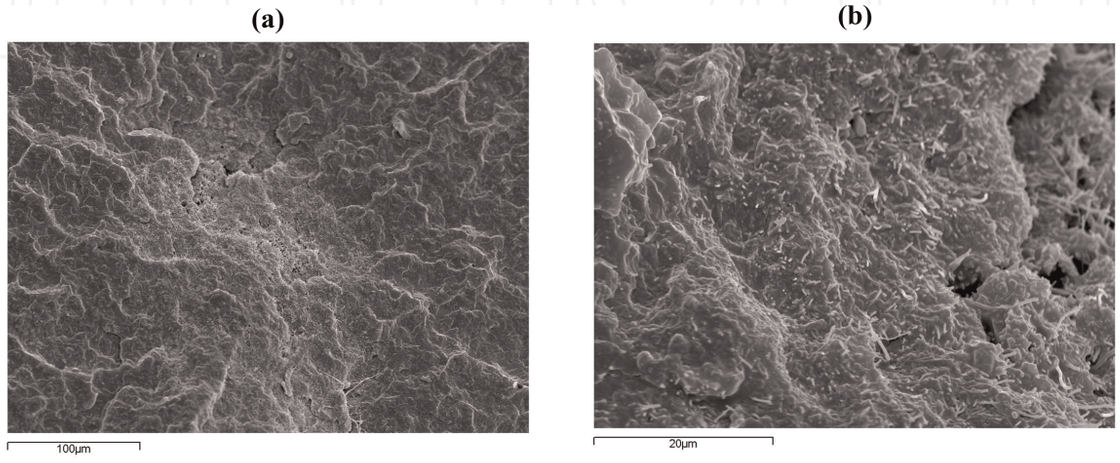

Figure 1.
Representative SEM micrographs of PP/CNF 2 wt. % composites: (a) low and (b) higher magnifications [13].

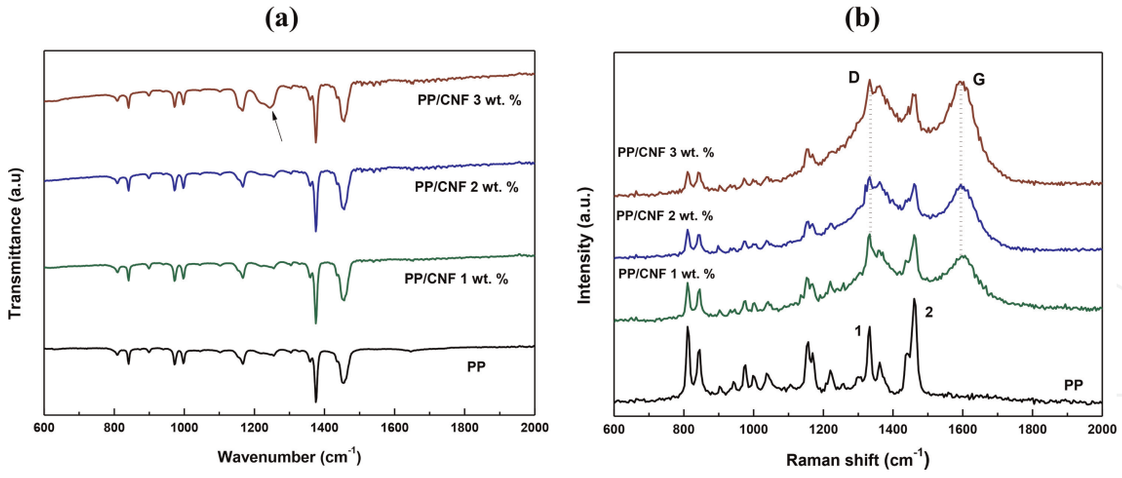

Figure 2.
PP/CNF composites: (a) FTIR and (b) Raman spectra (short dot lines are to guide the eye) [13].

The Raman spectra in 600–2000 cm^{-1} range of melt-extruded PP and PP/CNF composites are presented (**Figure 2b**). Polypropylene shows characteristic peaks in the range 800–1500 cm^{-1} [24], in accordance with the FTIR analysis (**Figure 2a**). Moreover, the intensity of the peaks corresponding to PP is reduced as the content of CNFs rises in PP/CNF composites. As expected, the PP/CNF composites show the G mode (1590 cm^{-1}), characteristic of graphitic lattice vibration of CNFs [25], and the D mode (1350 cm^{-1}), which corresponds to the disordered-induced band of CNFs [26]. It is noticed that the neat PP shows a Raman peak labeled with the number 1 (**Figure 2b**), which is overcome by the D band of CNFs in the PP/CNF composites. The peak position and the full-width half maximum (FWHM) of PP/CNF composites were determined by fitting the Raman spectra with Lorentzian functions. The calculated parameters together with the in-plane graphitic domain size (La) obtained according to L_a (nm) = 4.4 / (I_D/I_G) [27] are presented (**Table 1**). Notably, the $FWHM_G$, $FWHM_D$, and the G and D peak positions remained the same for all PP/CNF composites. The intensity ratios between the D and G bands (I_D/I_G) were also calculated and presented (**Table 1**). Again, La and the I_D/I_G ratios were identical for all PP/CNF composites. Both findings suggest that the degree of disorder of CNFs is not altered in PP/CNF composites. The intensity ratios (I_G/I_{PP}), between the amplitude of the G band corresponding to CNFs and one of the PP peaks present in all PP/CNF composites (~1464 cm^{-1}, marked with number 2 in **Figure 2b**) are also presented (**Table 1**). The ratio I_G/I_{PP} increases from 0.9 (PP/CNF 1 wt. %) to ~1.6 (PP/CNF 3 wt. %). Thus, it is confirmed that the content of CNFs in PP/CNF composites has increased.

PP/CNF	ω_G (cm^{-1})	$FWHM_G$ (cm^{-1})	ω_D (cm^{-1})	$FWHM_D$ (cm^{-1})	I_D/I_G	I_G/I_{PP} (2)	L_a(nm)
PP/CNF 1 wt. %	1598	95	1348	120	0,7	0,9	6,2
PP/CNF 2 wt. %	1598	95	1348	120	0,7	1,2	6,3
PP/CNF 3 wt. %	1598	95	1348	120	0,7	1,6	6,3

Table 1.
*Raman parameters of PP/CNF composites: D and G peak positions, full width half maximum, I_D/I_G, and I_G/I_{PP} (marked with 2 in **Figure 2b**) [13].*

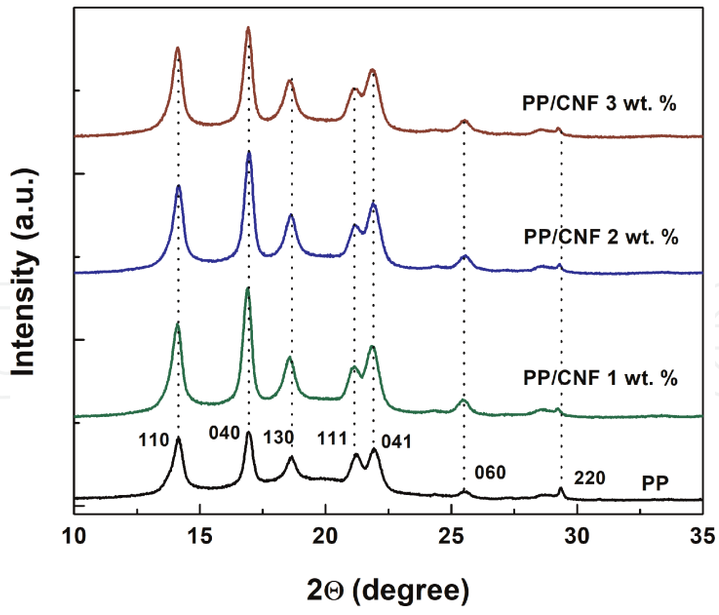

Figure 3.
XRD patterns of PP/CNF composites and position of lines due to the phase α of melt-extruded PP (short dot lines are to guide the eye) [12].

The XRD patterns of melt-extruded PP and PP filled with 1, 2, and 3 wt. % of CNFs are presented (**Figure 3**). PP shows a single phase α with peaks at 14.2° (110), 17.0° (040), 18.6° (130), 21.3° (111), 22.0° (041), 25.6° (060), and 28.9° (220) [28, 29]. Likewise, PP/CNF composites do not show substantive variations with reference to the XRD results of PP, an indication that CNFs do not contribute to the formation of other polypropylene phases. It must be noticed that the XRD peak located at 22° can be related to the diffraction line of CNFs [29]. It is worth mentioning that other works have related the peak at ~ 25.6° to the hexagonal crystals of graphite in CNTs [30].

3.2 AC conductivity

The experimental values of $\sigma'(\omega)$ and $\sigma''(\omega)$ at room temperature in the range from 430 to 2×10^6 Hz are represented (**Figure 4**). As expected, the $\sigma'(\omega)$ of PP/CNF

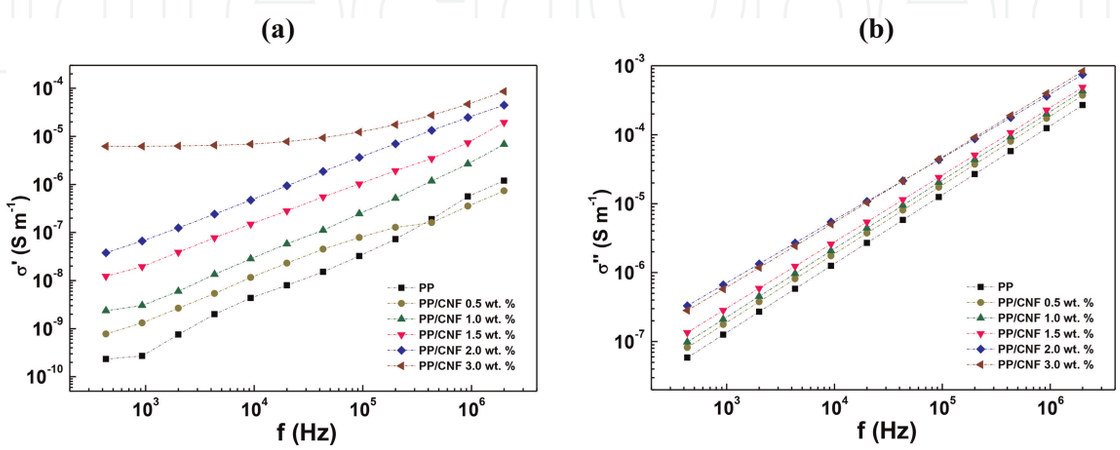

Figure 4.
AC complex conductivity versus frequency of PP/CNF composites: (a) σ′(ω) and (b) σ (ω). (Short dot lines are to guide the eye).

composites increases as a function of CNF loadings for all frequencies (**Figure 4a**). Moreover, it is evident that the $\sigma'(\omega)$ of unfilled PP and PP/CNF composites with up to 2 wt. % CNFs rises almost linearly with frequency over the entire frequency range. This latter behavior has been interpreted as conductivity through tunneling and hopping of electrons [31]. In contrast, the $\sigma'(\omega)$ of PP/CNF 3 wt. % composites (**Figure 4a**) exhibit two distinct profiles. At frequencies below ~ 20 kHz a frequency-independent regime is observed, while at high frequencies, $\sigma'(\omega)$ behaves like neat PP and PP/CNF composites with up to 2 wt. % CNFs. Thus, the $\sigma'(\omega)$ of PP/CNF 3 wt. % composites from 430 Hz to 20 kHz show evident signs of conductivity through direct contact between CNFs [32]. Similar to $\sigma'(\omega)$, the $\sigma''(\omega)$ of PP/CNF composites increases as a function of CNF loadings for all frequencies (**Figure 4b**). However, unlike $\sigma'(\omega)$, the $\sigma''(\omega)$ of PP/CNF composites shows always the same frequency-dependent behavior of unfilled PP. Interestingly, a small rise between 1.5 and 2 wt. % is found in $\sigma''(\omega)$, which can be attributed to the formation of conducting paths from 2 wt. % CNF loadings [33].

3.3 Dielectric permittivity

The frequency dependence of the dielectric permittivity of PP/CNF composites at room temperature in the range from 430 to 2×10^6 Hz is depicted (**Figure 5**). First of all, there is an evident increase of $\varepsilon'(\omega)$ as a function of CNF loadings for all frequencies in PP/CNF composites (**Figure 5a**) and, secondly the $\varepsilon'(\omega)$ of unfilled PP and PP/CNF composites with up to 1 wt. % CNFs is constant over the whole frequency range. This latter effect found in PP composites filled with 0.5 and 1 wt. % CNF loadings can be explained simply because the $\varepsilon'(\omega)$ of CNFs is much greater than that of unfilled PP [34]. However, as the amount of CNFs increases in the PP matrix, $\varepsilon'(\omega)$ becomes higher and frequency-dependent. In particular, $\varepsilon'(\omega)$ gradually changes from 2.4 for the PP to 12.9 for PP/CNF 3 wt. % composites at 1MHz. In this respect, the Maxwell-Wagner-Sillars (MWS) effect defined as the charge accumulation produced at the conductor-insulator interface is principally used in literature to explain the noticeable rise of $\varepsilon'(\omega)$ found in this type of carbon-based polymer composites at low frequencies [35]. On the contrary, the charge stored at the conductor-insulator interface is not able to respond to the electric field as the frequency rises, resulting in the decrease of $\varepsilon'(\omega)$ at higher frequencies (**Figure 5a**) [36]. On the other hand, the $\varepsilon''(\omega)$ (**Figure 5b**) is

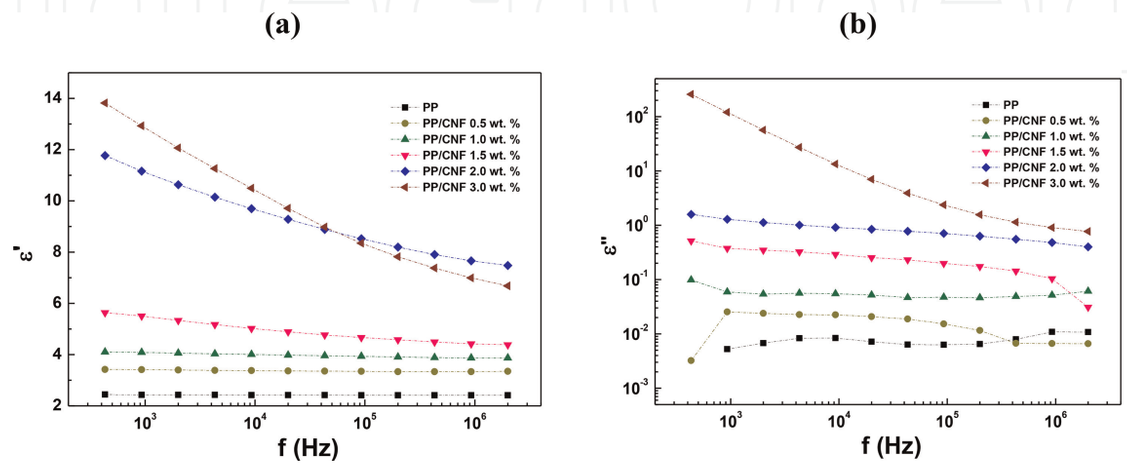

Figure 5.
Dielectric permittivity versus frequency of PP/CNF composites: (a) $\varepsilon'(\omega)$ and (b) $\varepsilon(\omega)$. (Short dot lines are to guide the eye).

frequency independent with an increase from 5×10^{-3} for PP to 1.29 for PP/CNF 2 wt. % composites at 1MHz. As expected from the $\varepsilon'(\omega)$ analysis, higher loadings of CNFs cause higher values of $\varepsilon''(\omega)$, and a change toward a frequency-dependent behavior at low frequencies due to the losses by electric conduction [37]. This is reflected in an increase of loss factor from 1.29 for PP/CNF 2 wt. % composites to 1.20×10^2 for PP/CNF 3 wt. % composites at 1MHz.

3.4 Electric modulus

The frequency dependence of the complex modulus of PP/CNF composites at room temperature in the range from 430 to 2×10^6 Hz is depicted (**Figure 6**). A decrease of $M'(\omega)$ is noticed as the content of CNFs increases in the PP. This $M'(\omega)$ reduction is connected with the enhanced dielectric permittivity achieved at higher loadings of CNFs (**Figure 5**). In addition, $M'(\omega)$ is practically constant over the whole range of frequencies for PP composites filled with 0.5 and 1 wt. % of CNFs. This constant value of $M'(\omega)$ is attributed to the inability of the large dipoles formed to follow the changes in the electric field [18]. The $M'(\omega)$ of PP/CNF 1.5 wt. % and 3 wt. % composites, for their part, show straight lines that increase slightly with the rise of frequency. This latter behavior can be linked to the increment of interfacial polarization caused by the higher contents of CNFs [38]. Notably, the existence of a step-wise increase in $M'(\omega)$ from low to high values of frequency in PP/CNF 2 wt. % composites imply a relaxation process, which is confirmed by the pronounced peaks of $M''(\omega)$ observed between 10^4 and 10^5 Hz (**Figure 6b**). This relaxation process confirms the existence of interfacial polarization in PP/CNF 2 wt. % composites [39]. Interestingly, the PP/CNF 3 wt. % composites do not show any peak in $M''(\omega)$, which can be associated with ohmic conduction losses that hinder the observation of relaxation process due to interfacial polarization in these PP/CNF 3 wt. % composites [40].

The Cole-Cole plots between the real and imaginary parts of electric modulus for PP/CNF 1.5, 2, and 3 wt. % composites are displayed (**Figure 7**) to complete the electrical modulus analysis [41]:

$$M^*(\omega) = M_\infty + \frac{M_S - M_\infty}{1 + (i\omega\tau)^{1-\alpha}} \tag{11}$$

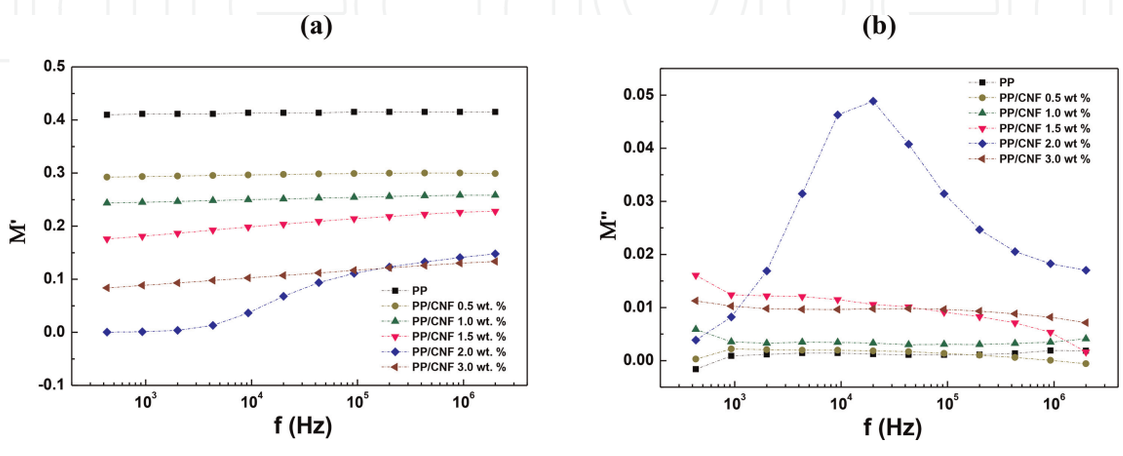

Figure 6.
Complex electric modulus versus frequency of PP/CNF composites: (a) $M'(\omega)$ and (b) $M(\omega)$. (Short dot lines are to guide the eye).

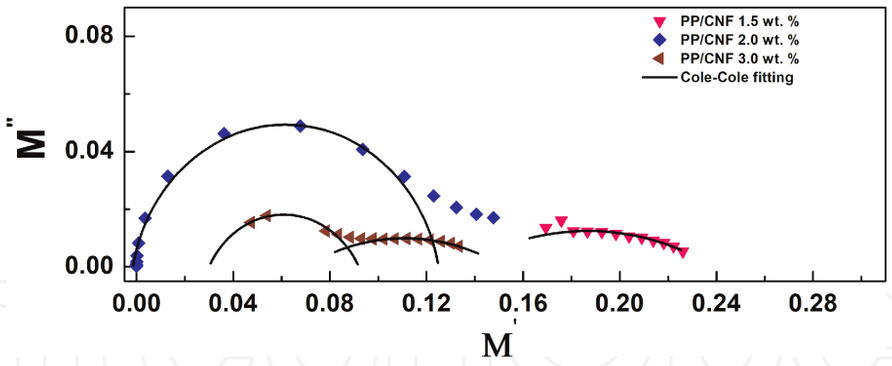

Figure 7.
Cole-Cole plot between the real M'(ω) and imaginary M (ω) parts of the electric modulus of PP/CNF composites. The black curves represent the fittings with Cole-Cole model by Eq. (11).

Sample	τ (μs)	(M_s–M_∞)	α
PP/CNF 1.5 wt. % (arc)	79.5	0.104	0.70
PP/CNF 2 wt. % (circle)	7.95	0.125	0.12
PP/CNF 3 wt. % (arc)	3.69	0.082	0.69
PP/CNF 3 wt. % (circle)	1700	0.049	0.10

Table 2.
Parameters τ, (M_S-M_∞) and α of PP/CNF composites extracted by the Cole-Cole model with Eq. (11).

Here, M_∞ is the modulus at high frequency, M_S is the static modulus, ω is the angular frequency, τ is the average relaxation time, and α is the dispersion coefficient, which takes values in the range (0–1). The relaxation curves of PP/CNF 1.5 wt. % composite represent a suppressed arc, while PP/CNF 2 wt. % and PP/CNF 3 wt. % composites show a suppressed semicircle shifted to the origin. In these latter cases, the displacement of semicircle toward the origin is attributed to the increase of τ with the larger heterogeneity of the system (**Table 2**) [42]. Moreover, the PP/CNF 2 wt. % composite shows a trend of forming a straight line at higher frequencies, which can be associated with conductance relaxation. Notably, two relaxation processes are clearly found in PP/CNF 3 wt. % composites. The first one represented by a suppressed circle and located closer to the origin reflects the bulk resistance of the sample, while the second one represented by a suppressed arc is due to interfacial polarization [39].

3.5 Electrical impedance

The Nyquist plots (Z´´ versus Z´) of PP and PP/CNF composites were analyzed to study the behavior of their relaxation frequency (**Figure 8**). As expected from the former sections, the plots of unfilled PP and PP composites with CNF contents from 0.5 to 2 wt. % (**Figure 8a**) are totally different from the plot of PP/CNF 3 wt. % composites (**Figure 8b**). In the first case, the response of PP is meanly capacitive, while as CNFs are added to PP, the introduction of the real component to the impedance leads to the formation of a semicircle [43], which is completely formed in PP/CNF 3 wt. % composite. This semicircle indicates the formation of conductive paths in these latter composites [44]. In particular, an equivalent circuit based on a resistor (R) in parallel with a constant phase element (CPE) can be utilized to model the complex impedance of this PP/CNF 3 wt. % composite. Thus, a constant R ~ 1.5×10^6 Ω and C

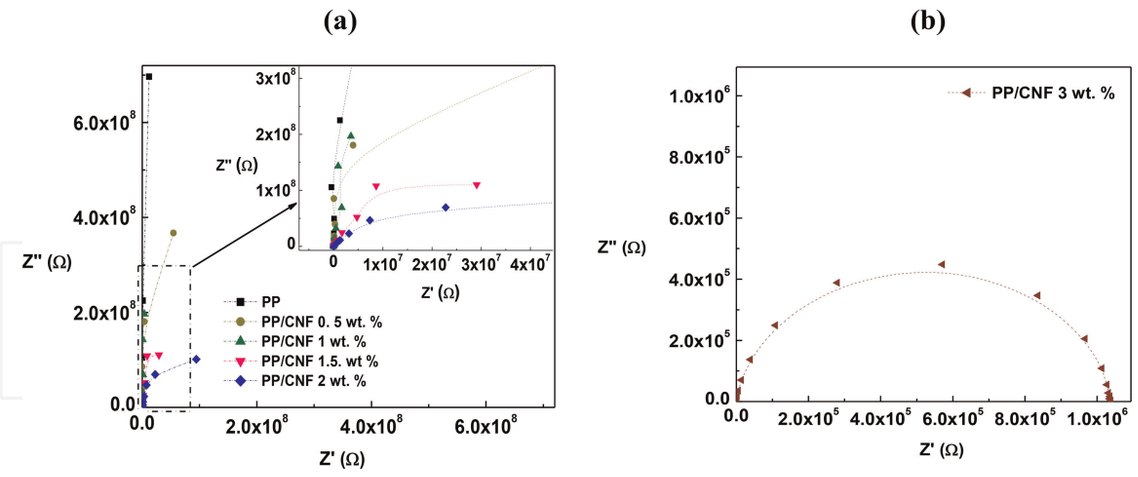

Figure 8.
Nyquist plots of the complex impedance of PP/CNF composites: (a) PP/CNF composites with up to 2 wt. % of CNFs and (b) PP/CNF 3 wt. % composites.

$\sim 1.4 \times 10^{-9}$ F below and above their characteristic frequency (9kHz), respectively, can be inferred as described in previous work [13].

4. Conclusion

Different weight contents of as-grown carbon nanofiber, produced by chemical vapor deposition and without any post-synthesis treatment, were melt-processed with polypropylene. The electrical conductivity of PP/CNF composites achieved values of $\sim 6 \times 10^{-6}$ S m^{-1} for PP/CNF 3 wt. % composites, which place them in the frontier between insulator and semiconductor materials. The values of conductivity correspond to a remarkable improvement of their dielectric permittivity due to the interfacial polarization between PP and CNFs. In addition, through the electrical modulus, the Cole–Cole model of PP/CNF composites is examined, from which is deduced that the incorporation of CNFs increases their heterogeneity and relaxation times. The aim of this study is to fill out the lack of works focused on the electric properties of PP composites filled with CNFs grown by CVD, but without any kind of post-treatment to improve their miscibility with polymers in the melt state.

Acknowledgements

This research was funded by the project UID/CTM/00264/2021 of 2C2T under the COMPETE and FCT/MCTES (PIDDAC) co-financed by FEDER through the PT2020 program.

Author details

António Jose Paleo[1*], Zineb Samir[2], Najoia Aribou[2], Yassine Nioua[2], Joaquim Agostinho Moreira[3] and Mohammed Essaid Achour[2*]

1 2C2T—Centro de Ciência e Tecnologia Têxtil, Universidade do Minho, Campus de Azurém, Guimarães, Portugal

2 Faculty of Sciences, Laboratory of Material Physics and Subatomic, Ibn Tofail University, Kenitra, Morocco

3 Faculdade de Ciências da Universidade do Porto, IFIMUP—Institute of Physics for Advanced Materials, Nanotechnology and Photonics and Departamento de Física e Astronomia, Porto, Portugal

*Address all correspondence to: ajpaleovieito@2c2t.uminho.pt and me.achour@uit.ac.ma

References

[1] Gogoi R, Kumar N, Mireja S, Ravindranath SS, Manik G, Sinha S. Effect of hollow glass microspheres on the morphology, rheology and crystallinity of short Bamboo fiber-reinforced hybrid polypropylene composite. Journal of Metals. 2019;**71**(2): 548-558. DOI: 10.1007/s11837-018-3268-3

[2] Gogoi R, Maurya AK, Manik G. A review on recent development in carbon fiber reinforced polyolefin composites. Composites Part C: Open Access. 2022;**8**: 100279. DOI: 10.1016/j.jcomc.2022.100279

[3] Anis Sofiah MK, Lin OH, Akil HM, Villagracia AR. Effect of compatibiliser on the accelerated weathering performance of polypropylene–silica nanocomposites. Materials Research Innovations. 2014;**18**(6):43-48

[4] Luo J, Cerretti G, Krause B, Zhang L, Otto T, Jenschke W, et al. Polypropylene-based melt mixed composites with singlewalled carbon nanotubes for thermoelectric applications: Switching from p-type to n-type by the addition of polyethylene glycol. Polymer. 2017;**108**:513-520. DOI: 10.1016/j.polymer.2016.12.019

[5] Tessonnier J-P, Rosenthal D, Hansen TW, Hess C, Schuster ME, Blume R, et al. Analysis of the structure and chemical properties of some commercial carbon nanostructures. Carbon. 2009;**47**(7):1779-1798. DOI: 10.1016/j.carbon.2009.02.032

[6] Aldica GV, Ciurea ML, Chipara DM, Lepadatu AM, Lozano K, Stavarache I, et al. Isotactic polypropylene–vapor grown carbon nanofibers composites: Electrical properties. Journal of Applied Polymer Science. 2017;**134**(38):1002

[7] Burton DJ, Glasgow DG, Lake ML, Kwag C, Finegan JC. Influence of carbon nanofibers surface characteristics on composite properties. In: Proceedings of the 46th International SAMPE Symposium and Exhibition. Long Beach, CA; 2001

[8] Gordeyev SA, Macedo FJ, Ferreira JA, van Hattum FWJ, Bernardo CA. Transport properties of polymer-vapour grown carbon fibre composites. Physica B: Condensed Matter. 2000;**279**(1-3): 33-36. DOI: 10.1016/S0921-4526(99)00660-2

[9] Lozano K, Bonilla-Rios J, Barrera EV. A study on nanofiber-reinforced thermoplastic composites (II): Investigation of the mixing rheology and conduction properties. Journal of Applied Polymer Science. 2001;**80**(8): 1162-1172. DOI: 10.1002/app.1200

[10] Aldica GV, Ciurea ML, Chipara DM, Lepadatu AM, Lozano K, Stavarache I, et al. Isotactic polypropylene–vapor grown carbon nanofibers composites: Electrical properties. Journal of Applied Polymer Science. 2017;**134**(38):45297. DOI: 10.1002/app.45297

[11] Muñoz-Ávila JM, Sánchez-Valdes S, Yáñez-Flores I, Rodriguez-Fernandez OS, Neira-Velázquez MG, Hernández-Hernández E, et al. Influence of carbon nanofiber functionalization and compatibilizer on the physical properties of carbon nanofiber reinforced polypropylene nanocomposites. Polymer Composites. 2018;**39**(10):3575-3585. DOI: 10.1002/pc.24380

[12] Paleo AJ, Aribou N, Nioua Y, Samir Z, Fernandes L, Moreira JA, et al. Electrical properties of melt-mixed polypropylene and as-grown carbon nanofiber composites: Analysis of their

interphase via the AC conductivity modeling. Journal of Composite Materials. 2022;**56**(12):1879-1889. DOI: 10.1177/00219983221084407

[13] Paleo AJ, Samir Z, Aribou N, Nioua Y, Martins MS, Cerqueira MF, et al. Dielectric spectroscopy of melt-extruded polypropylene and as-grown carbon nanofiber composites. The European Physical Journal E. 2021;**44**(5): 73. DOI: 10.1140/epje/s10189-021-00079-w

[14] Tibbetts GG, Doll GL, Gorkiewicz DW, Moleski JJ, Perry TA, Dasch CJ, et al. Physical properties of vapor-grown carbon fibers. Carbon. 1993;**31**(7):1039-1047. DOI: 10.1016/0008-6223(93)90054-E

[15] Lawrence JG, Berhan LM, Nadarajah A. Structural transformation of vapor grown carbon nanofibers studied by HRTEM. Journal of Nanoparticle Research. 2008;**10**(7): 1155-1167. DOI: 10.1007/s11051-007-9341-4

[16] Cortés P, Lozano K, Barrera EV, Bonilla-Rios J. Effects of nanofiber treatments on the properties of vapor-grown carbon fiber reinforced polymer composites. Journal of Applied Polymer Science. 2003;**89**(9):2527-2534. DOI: 10.1002/app.12309

[17] Paleo AJ, Sencadas V, Van Hattum FWJ, Lanceros-Méndez S, Ares A. Carbon nanofiber type and content dependence of the physical properties of carbon nanofiber reinforced polypropylene composites. Polymer Engineering and Science. 2014; **54**(1):117-128. DOI: 10.1002/pen.23539

[18] Tsangaris GM, Psarras GC, Kouloumbi N. Electric modulus and interfacial polarization in composite polymeric systems. Journal of Materials Science. 1998;**33**(8):2027-2037. DOI: 10.1023/A:1004398514901

[19] Sharma S, Basu T, Shahee A, Singh K, Lalla NP, Sampathkumaran EV. Complex dielectric and impedance behavior of magnetoelectric Fe2TiO5. Journal of Alloys and Compounds. 2016; **663**:289-294. DOI: 10.1016/j.jallcom.2015.12.090

[20] Jonscher AK. Dielectric relaxation in solids. Journal of Physics D: Applied Physics. 1999;**32**(14):R57-R70

[21] Al-Saleh MH, Sundararaj U. A review of vapor grown carbon nanofiber/polymer conductive composites. Carbon. 2009;**47**(1):2-22. DOI: 10.1016/j.carbon.2008.09.039

[22] Khafagy RM, Badr YA. In situ FTIR spectroscopic study of the recently detected low-temperature-induced structural changes in isotactic polypropylene. Journal of Polymer Science, Part B: Polymer Physics. 2005; **43**(20):2829-2842. DOI: 10.1002/polb.20567

[23] Chibani N, Djidjelli H, Dufresne A, Boukerrou A, Nedjma S. Study of effect of old corrugated cardboard in properties of polypropylene composites: Study of mechanical properties, thermal behavior, and morphological properties. Journal of Vinyl & Additive Technology. 2016;**22**(3):231-238. DOI: 10.1002/vnl.21437

[24] Nielsen AS, Pyrz R. A Raman study into the effect of transcrystallisation on thermal stresses in embedded single fibres. Journal of Materials Science. 2003;**38**(3):597-601. DOI: 10.1023/A:1021866429394

[25] Wang Y, Alsmeyer DC, McCreery RL. Raman spectroscopy of carbon materials: Structural basis of

observed spectra. Chemistry of Materials. 1990;**2**(5):557-563. DOI: 10.1021/cm00011a018

[26] Lehman JH, Terrones M, Mansfield E, Hurst KE, Meunier V. Evaluating the characteristics of multiwall carbon nanotubes. Carbon. 2011;**49**(8):2581-2602. DOI: 10.1016/j.carbon.2011.03.028

[27] Knight DS, White WB. Characterization of diamond films by Raman spectroscopy. Journal of Materials Research. 1989;**4**(2):385-393. DOI: 10.1557/JMR.1989.0385

[28] Zheng W, Lu X, Toh CL, Zheng TH, He C. Effects of clay on polymorphism of polypropylene in polypropylene/clay nanocomposites. Journal of Polymer Science, Part B: Polymer Physics. 2004; **42**(10):1810-1816. DOI: 10.1002/polb.20043

[29] Chipara M, Hamilton J, Chipara AC, George T, Chipara DM, Ibrahim EE, et al. Fourier transform infrared spectroscopy and wide-angle X-ray scattering: Investigations on polypropylene-vapor-grown carbon nanofiber composites. Journal of Applied Polymer Science. 2012;**125**(1):353-360. DOI: 10.1002/app.35576

[30] Ganß M, Satapathy BK, Thunga M, Weidisch R, Pötschke P, Jehnichen D. Structural interpretations of deformation and fracture behavior of polypropylene/multi-walled carbon nanotube composites. Acta Materialia. 2008;**56**(10):2247-2261. DOI: 10.1016/j.actamat.2008.01.010

[31] Al-Saleh MH. Influence of carbon nanotubes purity on the properties of carbon nanotubes/low-density polyethylene composites. Journal of Macromolecular Science, Part B. 2022:1-11. DOI: 10.1080/00222348.2022.2090049

[32] Taj M, Manohara SR. Significantly enhanced electrical and dielectric properties, and thermal stability of poly (3,4-ethylenedioxythiophene) coated on functionalized multiwalled carbon nanotubes. Synthetic Metals. 2020;**269**: 116572. DOI: 10.1016/j.synthmet.2020.116572

[33] Barnoss S, Aribou N, Nioua Y, El Hasnaoui M, Achour ME, Costa LC. Dielectric Properties of PMMA/PPy Composite Materials. Dordrecht: Springer; 2020

[34] Barick AK, Tripathy DK. Effect of nanofiber on material properties of vapor-grown carbon nanofiber reinforced thermoplastic polyurethane (TPU/CNF) nanocomposites prepared by melt compounding. Composites Part A: Applied Science and Manufacturing. 2010;**41**(10):1471-1482. DOI: 10.1016/j.compositesa.2010.06.009

[35] Shehzad K, Dang Z-M, Ahmad MN, Sagar RUR, Butt S, Farooq MU, et al. Effects of carbon nanotubes aspect ratio on the qualitative and quantitative aspects of frequency response of electrical conductivity and dielectric permittivity in the carbon nanotube/polymer composites. Carbon. 2013;**54**: 105-112. DOI: 10.1016/j.carbon.2012.10.068

[36] Alam RB, Ahmad MH, Islam MR. Effect of MWCNT nanofiller on the dielectric performance of bio-inspired gelatin based nanocomposites. RSC Advances. 2022;**12**(23):14686-14697. DOI: 10.1039/D2RA01508K

[37] Chang J, Liang G, Gu A, Cai S, Yuan L. The production of carbon nanotube/epoxy composites with a very high dielectric constant and low dielectric loss by microwave curing. Carbon. 2012;**50**(2):689-698. DOI: 10.1016/j.carbon.2011.09.029

[38] Singha S, Thomas MJ, Kulkarni A. Complex permittivity characteristics of epoxy nanocomposites at low frequencies. IEEE Transactions on Dielectrics and Electrical Insulation. 2010;**17**(4):1249-1258. DOI: 10.1109/TDEI.2010.5539697

[39] Bin-Dahman OA, Rahaman M, Khastgir D, Al-Harthi MA. Electrical and dielectric properties of poly(vinyl alcohol)/starch/graphene nanocomposites. The Canadian Journal of Chemical Engineering. 2018;**96**(4): 903-911. DOI: 10.1002/cjce.22999

[40] Samir Z, El Merabet Y, Graça M, Soreto Teixeira S, Achour M, Costa L. Dielectric behaviour of carbon nanotubes particles-filled polyester polymer composites. Journal of Composite Materials. 2017;**51**(13):1831-1837. DOI: 10.1177/0021998316665682

[41] Cole KS, Cole RH. Dispersion and absorption in dielectrics II. Direct current characteristics. The Journal of Chemical Physics. 1942;**10**(2):98-105. DOI: 10.1063/1.1723677

[42] Tsangaris GM, Psarras GC, Kontopoulos AJ. Dielectric permittivity and loss of an aluminum-filled epoxy resin. Journal of Non-Crystalline Solids. 1991;**131**:131-133

[43] Bowen CR, Buschhorn S, Adamaki V. Manufacture and characterization of conductor-insulator composites based on carbon nanotubes and thermally reduced graphene oxide. Pure and Applied Chemistry. 2014;**86**(5):765-774. DOI: 10.1515/pac-2013-1207

[44] Wang B, Liang G, Jiao Y, Gu A, Liu L, Yuan L, et al. Two-layer materials of polyethylene and a carbon nanotube/cyanate ester composite with high dielectric constant and extremely low dielectric loss. Carbon. 2013;**54**:224-233